Statistical equilibrium of bubble oscillations in dilute bubbly flows

Tim Colonius,[1] Rob Hagmeijer,[2] Keita Ando,[1] and Christopher E. Brennen[1]
[1]*California Institute of Technology, Pasadena, California 91125, USA*
[2]*Department of Mechanical Engineering, University of Twente, 7500 AE Enschede, The Netherlands*

(Received 12 October 2007; accepted 18 January 2008; published online 30 April 2008)

The problem of predicting the moments of the distribution of bubble radius in bubbly flows is considered. The particular case where bubble oscillations occur due to a rapid (impulsive or step change) change in pressure is analyzed, and it is mathematically shown that in this case, inviscid bubble oscillations reach a stationary statistical equilibrium, whereby phase cancellations among bubbles with different sizes lead to time-invariant values of the statistics. It is also shown that at statistical equilibrium, moments of the bubble radius may be computed using the period-averaged bubble radius in place of the instantaneous one. For sufficiently broad distributions of bubble equilibrium (or initial) radius, it is demonstrated that bubble statistics reach equilibrium on a time scale that is fast compared to physical damping of bubble oscillations due to viscosity, heat transfer, and liquid compressibility. The period-averaged bubble radius may then be used to predict the slow changes in the moments caused by the damping. A benefit is that period averaging gives a much smoother integrand, and accurate statistics can be obtained by tracking as few as five bubbles from the broad distribution. The period-averaged formula may therefore prove useful in reducing computational effort in models of dilute bubbly flow wherein bubbles are forced by shock waves or other rapid pressure changes, for which, at present, the strong effects caused by a distribution in bubble size can only be accurately predicted by tracking thousands of bubbles. Some challenges associated with extending the results to more general (nonimpulsive) forcing and strong two-way coupled bubbly flows are briefly discussed. © *2008 American Institute of Physics*.
[DOI: 10.1063/1.2912517]

I. INTRODUCTION

This paper is concerned with the computation of continuum models for bubbly flows. Mixture-averaged equations describing the motion (mixture density and velocity) and bubble dynamics (bubble radius and radial velocity) in such a flow have been derived by Zhang and Prosperetti[1] using a ensemble phase-averaging approach. The equations are closed in the dilute limit by specification of a probability density function (PDF) for the number of bubbles with a given radius and radial velocity.[2] For spherical bubbles initially in static equilibrium, the only uncertain quantity is the bubble equilibrium radius R_0. Once a probability distribution function for R_0 has been specified, a closed set of equations is obtained describing conservation of mass, bubble number density, momentum in the mixture, and equations describing the bubble dynamics. Most generally, the latter consists of a set of partial differential equation (PDE) describing conservation of mass, momentum, and energy inside the (spherical) bubble and at the interface, but with additional approximations, these are typically simplified to one or more ordinary differential equations (ODEs). In many cases, the model takes the form of the Rayleigh–Plesset equation or one of its generalizations.

With minor variations, this mixture-averaged model for bubbly flow was derived by earlier investigators[3–5] and has been used to investigate linear and nonlinear wave propagations in bubbly liquids.[6] For example, Commander and Prosperetti[7] provided a detailed comparison of the dispersion relation for small amplitude pressure waves with experimental data. Provided the distribution of bubble sizes is sufficiently broad, they found reasonable agreement for volume fractions up to a few percent. Nonlinear versions of the model have been used to investigate the structure of bubbly shock waves (e.g., Ref. 8), the dynamics of a cloud of bubbles subjected to a (spatially uniform) change in ambient pressure,[9–12] and cavitating nozzle flow,[13–15] and to model the dynamics of a cloud of bubbles excited by a focused shock wave in a lithotripter.[16]

Except for bubbly shock waves, comparison of the nonlinear models with experiments is limited and for the most part qualitative. Even so, the results make it clear that several features of the model warrant improvement. For example, Wang[14] showed that using a broad distribution of bubble sizes has a profound impact on the dynamics of bubbly flow in a converging-diverging nozzle. Indeed, when narrow distributions of bubbles are used, the nonlinear models are not self-consistent: Bubble dynamics can lead to rapid spatial variations in mixture-averaged properties that, in turn, may violate the modeling assumptions leading to the development of the internal bubble model. For example, it is often assumed that the mixture-averaged flow varies on a length scale that is long compared to the bubble, so that the bubble sees a locally uniform flow.

Unfortunately, the only available technique for computing flows with a distribution of bubbles sizes is a direct one whereby an extended Rayleigh–Plesset equation is solved at each point in space and for every possible equilibrium radius. Bubbles that oscillate on a time scale that is short com-

pared to the mixture-averaged time scale give rise to an oscillatory behavior of the PDF of the bubble radius. The direct approach becomes prohibitively expensive, as we show below, because many thousands of values of R_0 need to be tracked to accurately compute the average bubble radius and its variance. In this paper, we try to develop computationally efficient methods to accurately track bubble statistics. In order to simplify the presentation, we consider here the case of one-way coupling between the flow and the bubbles. That is, we assume that the pressure distribution in the continuous phase is given *a priori*. The principal result is that in many cases of interest, it is sufficient to track only a few bubbles, provided that the individual bubble radius is appropriately filtered (in time) prior to computing the required statistics.

In the next section, we formulate the mathematical problem and discuss the specific bubble models used in the following sections. In Sec. III, we demonstrate the existence, in the absence of forcing and viscous effects, of a statistical equilibrium, whereby phase cancellations among bubbles with different sizes lead to time-invariant values of the statistics. We show that at statistical equilibrium, moments of the distribution computed with the instantaneous bubble radius are equivalent to those computed by first period averaging the bubble radius. This averaging removes, to the extent possible, the oscillatory behavior in the integrand for the moments of the bubble radius and allows the bubble statistics to be accurately computed by tracking only a few bubbles. In Sec. IV, it is observed that, for typical broad equilibrium radius distributions, the time scale associated with relaxation to statistical equilibrium is short when compared to time scales associated with physical damping of bubble oscillations due to viscosity, compressibility, and heat transfer. This allows for a slowly varying statistical equilibrium that accounts for physical damping. A discussion of the results and prospects for their extension to continually forced bubbles (and ultimately two-way-coupled bubbly flows) is discussed in Sec. V.

II. BUBBLE MODELS

A. Preliminaries

In what follows, we normalize all length scales (including bubble radius and equilibrium radius) by a reference equilibrium radius (representing a probable bubble size) R_0^{ref}. Ambient liquid density ρ_0 and pressure p_0 are used to form mass and time scales so that, for example, time is normalized by $R_0^{\mathrm{ref}}\sqrt{\rho_0/p_0}$. This time scale is roughly a tenth of the period corresponding to the natural frequency of a bubble with equilibrium radius R_0^{ref}. Table I gives dimensional values of the time scale and natural period for reference bubble sizes of 1, 10, and 100 μm for an air bubble in water at 293 K. Nondimensional parameters governing the bubble dynamics are a Weber-like number $\hat{S}$, a Reynolds number Re, and a cavitation number Ca, which are defined by

$$\hat{S}=\frac{p_0 R_0^{\mathrm{ref}}}{S},\quad \mathrm{Re}=\sqrt{\frac{p_0}{\rho_0}}\frac{R_0^{\mathrm{ref}}}{\nu_0},\quad \mathrm{Ca}=\frac{p_0-p_v}{p_0}, \tag{1}$$

respectively, where ν_0, S, and p_v are the liquid kinematic viscosity, surface tension, and vapor pressure at ambient conditions. For water at 293 K, Ca=0.977, and values for the other nondimensional parameters are given for different bubble sizes in Table I. For the one-way coupling discussed here, the PDF for the equilibrium radius does not depend on the spatial position or time. We let $f(R_0)dR_0$ represent the probability of finding a bubble with equilibrium radius between R_0 and R_0+dR_0. Our main interest is, for a given bubble model, the evolution of moments of the bubble radius,

TABLE I. Time scales and nondimensional parameters for different equilibrium radii, all for air/water-vapor bubbles in water at 293 K. The table includes parameters for the model including heat transfer and liquid compressibility given in the Appendix. For bubbles of any size, Ca=0.977.

R_0^{ref} (μm)	1	10	100
Time scale $R_0^{\mathrm{ref}}\sqrt{\rho_0/p_0}$ (s)	10^{-7}	10^{-6}	10^{-5}
Natural period (s)	6.7×10^{-7}	9.3×10^{-6}	9.7×10^{-5}
Re	10	10^2	10^3
$\hat{S}$	1.39	13.9	139.3
Pe_T	1.16	5.50	48.8
Pe_χ	0.416	4.16	41.6

$$\mu_m(t)=\int_0^\infty R(t;R_0)^m f(R_0)dR_0. \tag{2}$$

For example, the mean radius $[\mu_1(t)]$ and the mean bubble volume $[\mu_3(t)]$ both appear in the ensemble phase-averaged equations for a bubbly flow.

We illustrate specific examples with a lognormal distribution,

$$f(R_0)=\frac{1}{\sqrt{2\pi}\sigma R_0}e^{-\ln^2(R_0)/2\sigma^2}, \tag{3}$$

where σ is the standard deviation of the log of the equilibrium radius. The measured distributions in water tunnels and for naturally occurring bubble nuclei in seawater[17] show considerable scatter but are reasonably fit by the lognormal distribution with $R_0^{\mathrm{ref}}\approx 10$ μm and $\sigma\approx 0.7$.

B. Rayleigh–Plesset equation

The simplest model we consider is the Rayleigh–Plesset equation for a bubble with a spatially uniform mixture of noncondensable gas and vapor. The gas is assumed to be adiabatically compressed. The usual derivation[17] gives

$$R\ddot{R}+\frac{3}{2}\dot{R}^2+\frac{4}{\mathrm{Re}}\dot{R}R^{-1}=F(R,R_0,C_p), \tag{4}$$

where R is the bubble radius and $\dot{R}$ and $\ddot{R}$ are the first and second time derivatives of R, respectively. Furthermore, $C_p(t)=[p_\infty(t)-p_0]/p_0$ is the specified distribution of pressure in the continuous phase (i.e., far from the bubble), and

$$F(R,R_0,C_p) = -\frac{2}{\hat{S}R_0}\left\{\left(\frac{R}{R_0}\right)^{-1} - \left(\frac{R}{R_0}\right)^{-3\gamma}\right\} + \mathrm{Ca}\left(\frac{R}{R_0}\right)^{-3\gamma} - \{C_p(t) + \mathrm{Ca}\}. \quad (5)$$

It is noted that throughout the paper, the dependency of functions on $\hat{S}$ and Ca is not explicitly written.

When $\mathrm{Re}\to\infty$ and $\dot{C}_p=0$, then trajectories $(R,\dot{R})$ in phase space are described by curves of constant Hamiltonian.[18–20] We define the Hamiltonian as

$$\mathcal{H}(R,\dot{R},R_0,C_p) \equiv \tfrac{1}{2}R^3\dot{R}^2 + G(R,R_0,C_p) - G(R_{\mathrm{eq}},R_0,C_p), \quad (6)$$

where

$$G(R,R_0,C_p) \equiv \frac{2R_0^2}{\hat{S}}\left\{\frac{1}{2}\left(\frac{R}{R_0}\right)^2 + \frac{1}{3(\gamma-1)}\left(\frac{R}{R_0}\right)^{-3(\gamma-1)}\right\} + \mathrm{Ca}R_0^3\left\{\frac{1}{3}\left(\frac{R}{R_0}\right)^3 + \frac{1}{3(\gamma-1)}\left(\frac{R}{R_0}\right)^{-3(\gamma-1)}\right\} + \frac{1}{3}C_p(t)R^3. \quad (7)$$

In Eq. (6), we have used the pressure-dependent equilibrium radius, $R_{\mathrm{eq}}(R_0,C_p)$, which is implicitly defined by

$$F(R_{\mathrm{eq}},R_0,C_p) = 0, \quad (8)$$

expressing that a bubble with $R=R_{\mathrm{eq}}(R_0,C_p)$ is stationary at that particular value of C_p. We note that R_0, which is used in this paper to label individual bubbles, is the equilibrium radius at $C_p=0$, i.e., $R_{\mathrm{eq}}(R_0,0)=R_0$. The first term in Eq. (6) is the kinetic energy of the liquid surrounding the bubble,[21] whereas the function G can be interpreted as being the potential energy corresponding to the force field $-FR^2$ that drives the oscillation:

$$\frac{\partial G}{\partial R} = -FR^2. \quad (9)$$

Hence, $\mathcal{H}$ represents the total energy of the bubble and its surrounding liquid, which is zero when $(R,\dot{R})=(R_{\mathrm{eq}},0)$. It is easily verified that upon setting $q=R$ and $p=R^3\dot{R}$, we obtain the following differential equations:

$$\dot{q} = \frac{\partial\mathcal{H}}{\partial p},$$

$$\dot{p} = -\frac{\partial\mathcal{H}}{\partial q} - \frac{4}{\mathrm{Re}}pq^{-2}, \quad (10)$$

$$\dot{\mathcal{H}} = -\frac{4}{\mathrm{Re}}p^2q^{-5} + \frac{1}{3}(q^3 - q_{\mathrm{eq}}^3)\dot{C}_p.$$

The third expression confirms that deviations from Hamiltonian trajectories are caused by (a) viscous damping ($\mathrm{Re}<\infty$), always leading to loss of energy, and (b) pressure variations ($\dot{C}_p\neq 0$), which may either decrease energy or increase energy depending on the signs of $q^3-q_{\mathrm{eq}}^3$ and $\dot{C}_p$. Indeed, when a pressure variation is applied such that $\mathrm{sign}(\dot{C}_p)=\mathrm{sign}(q-q_{\mathrm{eq}})$ at all times, i.e., when the pressure signal is resonant, the total energy will continuously grow.

Equation (10) shows that the bubble dynamics are Hamiltonian when $\mathrm{Re}\to\infty$ and $\dot{C}_p=0$. In that case, $\mathcal{H}$ is constant, and $\dot{R}^2$ is a function of R,

$$\tfrac{1}{2}\dot{R}^2 = \{\mathcal{H} - G(R,R_0,C_p) + G(R_{\mathrm{eq}},R_0,C_p)\}/R^3. \quad (11)$$

The minimum and maximum radii of this closed trajectory, $R_{\min}(R_0,C_p)$ and $R_{\max}(R_0,C_p)$, are the solutions (for R) of

$$G(R,R_0,C_p) - G(R_{\mathrm{eq}},R_0,C_p) = \mathcal{H}. \quad (12)$$

Consider cases where $|C_p|$ is small with the bubble radius close to R_0, then it is appropriate to linearize Eq. (4) about R_0. By denoting $R'=R-R_0$, we obtain

$$\ddot{R}' + 2\beta(R_0)\dot{R}' + \omega^2(R_0)R' = -C_p/R_0, \quad (13)$$

where

$$\beta(R_0) = \frac{2}{\mathrm{Re}R_0^2} \quad \text{and} \quad \omega^2(R_0) = \frac{3\gamma\mathrm{Ca}}{R_0^2} + \frac{2}{\hat{S}R_0^3}(3\gamma-1)$$

characterize the damping rate and bubble natural frequency, respectively. Suppose that all bubbles are initially in static equilibrium at $C_p=C_p^0$:

$$R'(t<0;R_0) = \epsilon R_0, \quad \epsilon = -\frac{C_p^0}{\omega^2R_0^2},$$

and that there is a rapid step change of pressure toward $C_p=0$. Then, in the limit of $\hat{S}\to\infty$, the value of ϵ is independent of R_0 and we can rescale the response to eliminate dependence on ϵ, i.e., let $R' := R'/\epsilon$ so that $R'(0)=R_0$. Since the value of $\omega^2-\beta^2$ is generally positive, the relevant solution is

$$R'(t;R_0) = R_0e^{-\beta(R_0)t}\cos\left[\sqrt{\omega^2(R_0) - \beta^2(R_0)^2}\,t\right]. \quad (14)$$

Evolution of the statistical moments of bubble radius is discussed later in Sec. III A. More general initial conditions for both the bubble radius and bubble radial velocity are discussed in Sec. III B 2.

C. Model including liquid compressibility and heat transfer

Some of the assumptions made in deriving the Rayleigh–Plesset equation, most notably the neglect of liquid compressibility and the assumption of polytropic compression/expansion of the bubble contents, need to be relaxed in order to obtain a realistic model for spherical bubble dynamics. Most generally, a set of PDEs describing radial transport of momentum, heat, and mass transfer need to be solved in the bubble and surrounding liquid. Needless to say, such computations for each bubble (and each possible bubble size) in a complex bubbly flow are prohibitively computationally intensive. Several models have been introduced that include heat and mass transfer in an approximate way and allow for the bubble radius to be computed by solving a few ODEs. It is beyond the scope of the present paper to discuss these models or their relative merits in detail; see (Refs. 22–29 for more details. Rather, our purpose is to show that the analysis of statistical equilibrium can be adapted from the Rayleigh–

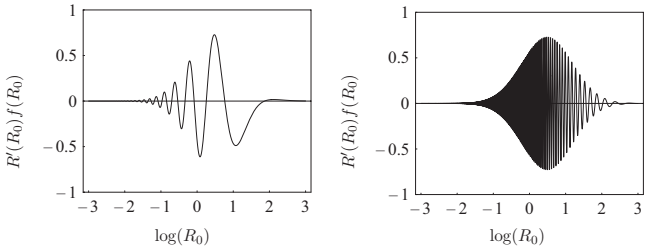

FIG. 1. The integrand of Eq. (15) for $\mu_1'(t)$ due to impulsive $C_p(t)$ at times $t=5$ (left) and $t=100$ (right) for linear, inviscid bubbles.

Plesset equation, for which it is derived, to more complex models of the bubble behaviors. For this purpose, we implement a model based on Gilmore's[30] generalization of the Rayleigh–Plesset equation which accounts, to first order, for effects of liquid compressibility, and we couple it to a reduced-order model proposed by Preston *et al.*[29] for the heat and mass transfer. The assumptions and equations for this model are given in the Appendix. Quantities such as bubble radius, pressure, and so on, are normalized as discussed in Sec. II A, and the two additional nondimensional parameters (Peclet numbers) needed to initialize the model are given in Table I.

III. STATISTICAL EQUILIBRIUM

In this section, we show, first by direct integration and then theoretically, that inviscid bubbles (viscosity, liquid compressibility, and heat transfer are ignored), which are in static equilibrium and then forced by an impulsive or step change in pressure, $C_p(t)$, reach a statistical equilibrium whereby the moments of the bubble radius become independent of time. The main theoretical results are (a) that the statistical equilibrium exists and (b) that moments of the distribution can be found by first averaging each bubble history over a period of oscillation. We show why the latter result leads to vast reduction in computational expense in computing the statistical equilibrium solutions when the bubble histories are determined by numerical integration.

A. Observations from direct computation

Starting with the linearized case, we consider bubbles that evolve from a nonequilibrium initial condition (which is in turn equivalent to the response to a pressure step change), according to Eq. (14). Similar results can be obtained with

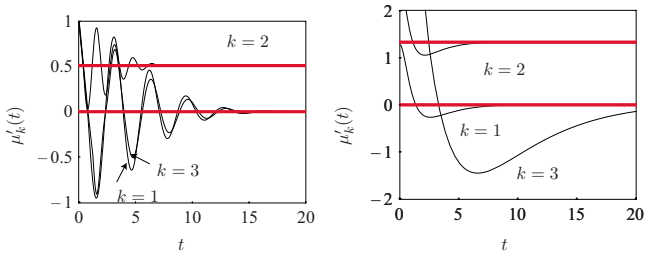

FIG. 2. (Color online) Moments of the bubble radius for impulsive $C_p(t)$ for $\sigma=0.1$ (left) and $\sigma=0.7$ (right) with linear, inviscid bubbles. The horizontal red lines indicate the theoretical limits for the moments derived in Sec. III C.

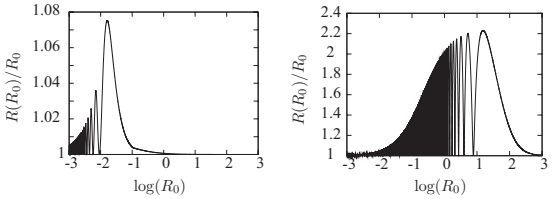

FIG. 3. The scaled radius for a step change in pressure with $C_p=-0.84$ Ca at times $t=10^{-2}$ (left) and $t=10^2$ (right) with nonlinear, inviscid bubbles.

more general (smooth) initial conditions for the bubble radius and radial velocity as discussed in Sec. III B 2. Here, we directly compute

$$\mu_m'(t) = \int_0^\infty [R'(t,R_0)]^m f(R_0) dR_0 \tag{15}$$

for the lognormal distribution with $R_0^{\mathrm{ref}}=10$ μm and various values of σ. The integrand is plotted for $m=1$ (average radius) in Fig. 1 at early and late times. The integrand becomes progressively more oscillatory for a large time due to the inverse proportionality between the natural frequency ω and the equilibrium radius. While the integral can be analytically evaluated in this case (discussed below), it is instructive to perform numerical integrations since in the general nonlinear case, the bubble motion can only be numerically computed. In Fig. 2, the first two moments are plotted for two values of σ. The behavior is to be expected: The broader the distribution, the more quickly cancellation between bubbles at different phases of their oscillation cycles occur, and the more rapidly the moments converge to a steady-state value. We term this "statistical equilibrium" to distinguish it from static equilibrium.

A similar behavior occurs for the nonlinear inviscid case. The scaled radius, R/R_0, is depicted in Fig. 3 at early and late times, and the evolution of the moments is plotted in Fig. 4. In this example, the bubbles are forced by a (negative) step change in pressure, which causes bubbles to follow Hamiltonian trajectories with minimum radius R_0. Note that in this case, the time dependent bubble radii, $R(t;R_0)$, were constructed from curves of constant Hamiltonian rather than direct time integration of the Rayleigh–Plesset equation. Again, a statistical equilibrium is achieved for a long time.

Several features of the nonlinear evolution are worth noting for future reference. Figure 3 shows that at $t=10^{-2}$, the smaller bubbles ($R_0<1$) are oscillating, whereas the larger bubbles ($R_0>1$) are still in their initial state. The largest peak represents a bubble that has reached its maximum

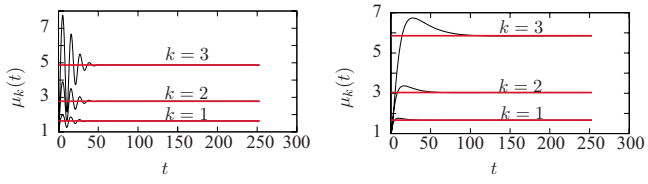

FIG. 4. (Color online) Moments of the bubble radius for a step decrease in pressure with $C_p=-0.84$ Ca for $\sigma=0.1$ (left) and $\sigma=0.7$ (right) with nonlinear, inviscid bubbles. The horizontal red lines indicate the theoretical limits for the moments derived in Sec. III D.

radius for the first time. The minimum left to it represents a bubble that has completed its trajectory for the first time, the next minimum represents a bubble that has completed its trajectory for the second time, and so on. When the minima are numbered from right to left, then the corresponding bubbles in terms of R_0 can be found from

$$T(R_{0,n}(t)) = t/n, \quad n = 1,2,3, \ldots, \tag{16}$$

where $T(R_0)$ represents the oscillation period of a bubble with R_0. Taylor expansion of $T(R_0)$ leads to

$$R_{0,n+1}(t) - R_{0,n}(t) = -\frac{T_n}{nT_n'} + \mathcal{O}\left(\frac{1}{n^2}\right), \tag{17}$$

where $T_n = T[R_{0,n}(t)]$ and $T_n' = T'[R_{0,n}(t)]$, which shows that the distance between two neighboring minima becomes arbitrarily small when $t/T(R_{0,n})$ becomes sufficiently large. At $t = 10^2$, the larger bubbles are also oscillating, and the $R_{0,n}(t)$ have increased. An implication of this result is that any quadrature of the integrand is destined (in the inviscid case) to fail for sufficiently long times no matter how many quadrature points are used.

B. Theory

1. Derivation of statistical equilibrium

We now show that the statistical equilibrium exists by considering an arbitrary but smooth functional $\Psi[R(t,R_0)]$, which is allowed to be a function of R and any of its time derivatives. The expectation of Ψ is

$$E(\Psi;t) = \int_0^\infty f(R_0)\Psi[R(t,R_0)]dR_0. \tag{18}$$

Since $\omega(R_0) \equiv 2\pi/T(R_0)$ is a strictly decreasing function of R_0, we can transform functions from the (t,R_0) plane to the (t,ω) plane,

$$\bar{R}[t,\omega(R_0)] = R(t,R_0),$$

$$\bar{f}[\omega(R_0)] = f(R_0), \tag{19}$$

$$dR_0 = \frac{dR_0}{d\omega}d\omega,$$

which gives

$$E(\Psi;t) = \int_0^\infty \bar{f}(\omega)\left|\frac{dR_0}{d\omega}\right|\Psi[\bar{R}(t,\omega)]d\omega. \tag{20}$$

In the inviscid, impulsively (or step-change) forced case, each bubble eventually oscillates periodically in time, so for a sufficiently large time, we can expand the function Ψ in a Fourier series,

$$\Psi[\bar{R}(t,\omega)] = \sum_{j=-\infty}^{\infty} \Psi_j(\omega)e^{ij\omega t}. \tag{21}$$

Upon substitution into Eq. (20), this leads to

$$E(\Psi;t) = \sum_{j=-\infty}^{\infty}\int_0^\infty \bar{f}(\omega)\left|\frac{dR_0}{d\omega}\right|\Psi_j(\omega)e^{ij\omega t}d\omega. \tag{22}$$

Provided that the PDF, $f(R_0)$, and all its derivatives vanish for $R_0 \to 0$ and $R_0 \to \infty$, the Riemann–Lebesgue theorem[31] implies that

$$\lim_{t\to\infty}\int_0^\infty \bar{f}(\omega)\left|\frac{dR_0}{d\omega}\right|\Psi_j(\omega)e^{ij\omega t}d\omega = 0, \quad j \neq 0, \tag{23}$$

$$\lim_{t\to\infty} E(\Psi;t) = \int_0^\infty \bar{f}(\omega)\left|\frac{dR_0}{d\omega}\right|\Psi_0(T)d\omega. \tag{24}$$

That is, the existence of the limit proves that statistical equilibrium is achieved in the general, nonlinear case.

A further result that is the key to efficient computation of the moments can be found by backtransformation and noting that

$$\Psi_0 = \frac{1}{T}\int_0^T \Psi[R(t,R_0)]dt. \tag{25}$$

This finally leads to an expression for the equilibrium expectation:

$$\lim_{t\to\infty} E(\Psi;t) = E(\Psi) = \int_0^\infty f(R_0)\left[\frac{1}{T(R_0)}\int_0^{T(R_0)}\Psi[R(t,R_0)]dt\right]dR_0. \tag{26}$$

Equation (26) shows that at statistical equilibrium, it is permissible to replace Ψ by its period-averaged value. The importance of this is made evident by comparing the integrand of Eq. (26), for $\Psi(R) = R$, with the integrand of the original expression for $\mu_1(t)$, viz., Eq. (2). The value of the integral has been shown to be identical, but the singular oscillatory behavior of the integrand has been removed in Eq. (26), thus allowing accurate numerical evaluation with relatively few quadrature points. This is demonstrated below.

Finally, we note that one can also verify Eq. (26) by first *supposing* that the system is in statistical equilibrium, in which case, $E(\Psi;t)$ is independent of t and equal to its time-averaged value:

$$E(\Psi,t) = \frac{1}{t}\int_0^t E(\Psi,t)dt = \int_0^\infty f(R_0)\left[\frac{1}{t}\int_0^t \Psi[R(t,R_0)]dt\right]dR_0. \tag{27}$$

For long times t, the properties of the Fourier integral are such that the long time average inside the integrand can be replaced by the integral over a single period $T(R_0)$, which again directly leads to Eq. (26).

2. More general initial conditions

Expression (26) does not explicitly depend on the initial conditions for the bubble radius $R(0)$ or radial velocity $\dot{R}(0)$, but application of the Riemann–Lebesgue theorem to Eq. (22) requires that the integrand be a smooth function of R_0 (and by transformation, ω). This, in turn, requires that the bubble response, $R[t,\omega(R_0)]$, and hence the initial conditions, $R(0)$ and $\dot{R}(0)$, be smooth functions of R_0. Conversely, provided the initial conditions are smooth, statistical equilibrium will be achieved and Eq. (26) will hold regardless of the particular initial conditions.

3. Equilibrium probability density function

We will derive an explicit expression for the PDF $f_r(r)$ in case of statistical equilibrium. Given a specific value of R_0, the fraction of the period that the bubble radius is smaller than r is

$$F(r,t;R_0)=\frac{1}{t}\int_0^t H[r-R(t;R_0)]dt, \tag{28}$$

with $H(r)$ the Heaviside step function. For large, random values of t, $F(r;R_0)$ represents the probability of the bubble radius being smaller than r. When $t/T(R_0)\to\infty$, the integral can be replaced by

$$F(r;R_0)=\frac{1}{T(R_0)}\int_0^{T(R_0)} H[r-R(t;R_0)]dt, \tag{29}$$

which leads to a corresponding conditional PDF,

$$f_{r|R_0}(r|R_0)=\frac{1}{T(R_0)}\int_0^{T(R_0)} \delta[r-R(t;R_0)]dt, \tag{30}$$

with $\delta(r)$ the Dirac delta function. Hence, the equilibrium PDF is

$$f_r(r)=\int_0^\infty f_{r|R_0}(r|R_0)f(R_0)dR_0. \tag{31}$$

To test the consistency of this expression with our previous statistical equilibrium results, it is easily verified that evaluation of

$$\int_0^\infty f_r(r)\Psi(r)dr \tag{32}$$

by changing the order of integration twice again leads to Eq. (26).

C. Application to linearized dynamics

To demonstrate our theory, we derive explicit expressions for the equilibrium moments and PDF for the linearized dynamics and compare these to expressions derived by direct computation. Setting $\mathrm{Re}\to\infty$, Eq. (14) becomes

$$R'(t;R_0)=R_0\cos[\omega(R_0)t]. \tag{33}$$

The corresponding moments are defined as

$$\mu_k'(t)=E(R'^k,t),\quad k\in\mathbb{N}. \tag{34}$$

For the equilibrium moments, we apply Eq. (26),

$$\frac{1}{T(R_0)}\int_0^{T(R_0)}\Psi[R(t,R_0)]dt=\frac{R_0^k}{\pi}\int_0^\pi \cos^k(\tau)d\tau=\begin{cases}0, & k \text{ odd},\\ \left(\dfrac{2R_0^k}{\pi}\right){}_2F_1\left(\dfrac{k+1}{2},\dfrac{1}{2};\dfrac{k+3}{2},1\right), & k \text{ even},\end{cases} \tag{35}$$

where ${}_2F_1$ is the hypergeometric function. We use

$${}_2F_1(a,b;c,1)=\frac{\Gamma(c)\Gamma(c-a-b)}{\Gamma(c-a)\Gamma(c-b)},\quad c-a-b>0, \tag{36}$$

to write

$${}_2F_1\left(\frac{k+1}{2},\frac{1}{2};\frac{k+3}{2},1\right)=\frac{\Gamma\left(\dfrac{k+3}{2}\right)\Gamma\left(\dfrac{1}{2}\right)}{\Gamma(1)\Gamma\left(\dfrac{k+2}{2}\right)}, \tag{37}$$

and with $\Gamma(\frac{1}{2})=\sqrt{\pi}$ and $\Gamma(1)=1$, we get

$$\mu_k'=\begin{cases}0, & k \text{ odd},\\ \dfrac{2}{\sqrt{\pi}(k+1)}\dfrac{\Gamma\left(\dfrac{k+3}{2}\right)}{\Gamma\left(\dfrac{k+2}{2}\right)}\displaystyle\int_0^\infty R_0^k f(R_0)dR_0, & k \text{ even}.\end{cases} \tag{38}$$

For the specific case when $f(R_0)$ is lognormal, we have

$$\int_0^\infty R_0^k f(R_0)dR_0=e^{(1/2)k^2\sigma^2}, \tag{39}$$

so for $k=0$ and $k=2$, we find

$$\mu_0'=1,\quad \mu_2'=\tfrac{1}{2}e^{2\sigma^2}. \tag{40}$$

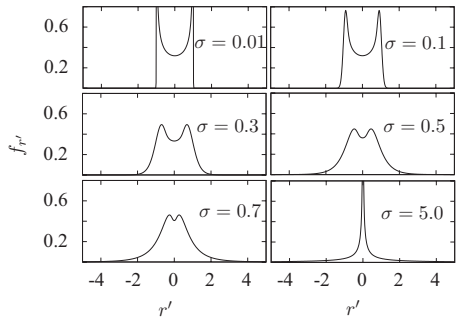

FIG. 5. Equilibrium PDF, $f'(r')$, for various values of σ and with $C_p = -0.84Ca$, for linear inviscid bubbles.

These values are identical to the directly computed statistical equilibrium as shown in Fig. 2.

To derive the equilibrium PDF, we calculate the integral given by Eq. (29), differentiate the result, and finally integrate over R_0. Substitution of Eq. (33) into Eq. (29) gives

$$F(r';R_0) = \begin{cases} 1, & r'/R_0 \geqslant 1, \\ 1 - (1/\pi)\arccos(r'/R_0), & -1 < r'/R_0 < 1, \\ 0, & r'/R_0 \leqslant -1, \end{cases} \tag{41}$$

which, upon differentiation with respect to r', leads to

$$f_{r'|R_0}(r'|R_0) = \begin{cases} 0, & |r'/R_0| \geqslant 1, \\ (1/\pi)(R_0^2 - r'^2)^{-1/2}, & |r'/R_0| < 1. \end{cases} \tag{42}$$

Finally, integration gives

$$f_{r'}(r') = \frac{1}{\pi}\int_{|r'|}^{\infty} \frac{1}{\sqrt{R_0^2 - r'^2}} f(R_0) dR_0. \tag{43}$$

For $r'=0$, the integral can be analytically found,

$$f_{r'}(0) = \pi^{-1} e^{(1/2)\sigma^2}. \tag{44}$$

For other values of r', we introduce $x = R_0 - |r'|$, write $R_0^2 - r'^2 = (R_0 + |r'|)(R_0 - |r'|)$, and integrate by parts to eliminate the singularity,

$$f_{r'}(r') = \frac{1}{\pi}\int_0^{\infty} \frac{f(x+|r'|) - 2f'(x+|r'|)(x+2|r'|)}{(x+2|r'|)^{3/2}} \sqrt{x}\, dx. \tag{45}$$

The remaining integral can be readily numerically evaluated. Figure 5 shows the typical results.

When moments of $f_{r'}$ are computed, it is convenient to rewrite Eq. (43) as

$$f_{r'}(r') = \frac{1}{\pi}\int_0^{\infty} \frac{H(R_0^2 - r'^2)}{\sqrt{R_0^2 - r'^2}} f(R_0) dR_0, \tag{46}$$

which enables one to interchange the order of integration, i.e.,

$$\int_{-\infty}^{\infty} r'^k f_{r'}(r') dr' = \frac{1}{\pi}\int_0^{\infty} f(R_0)\left[\int_{-R_0}^{R_0} \frac{r'^k}{\sqrt{R_0^2 - r'^2}} dr'\right] dR_0. \tag{47}$$

From this result, it is straightforward to recover μ_0' and μ_2' given by Eq. (40).

D. Application to nonlinear dynamics

When we solve the nonlinear Rayleigh–Plesset equation in the limit of $\mathrm{Re} \to \infty$ and $\dot{C}_p = 0$ in terms of closed curves of constant Hamiltonian in the $(R, \dot{R})$ space, the time coordinate is eliminated. To apply our statistical equilibrium model, it is therefore convenient to replace the time integrals by radius integrals. As long as $\dot{R} > 0$, we may invert $R(t)$ to $t(R)$ with

$$\frac{dt}{dR} = \dot{R}^{-1}, \tag{48}$$

and therefore, by using Eq. (11), we may transform Eq. (26) into

$$E(\Psi) = \int_0^{\infty} f(R_0)\left[\frac{2}{T(R_0)}\int_{R_{\min}}^{R_{\max}} \Psi(R)\dot{R}^{-1} dR\right] dR_0, \tag{49}$$

with

$$T(R_0) = 2\int_{R_{\min}}^{R_{\max}} \dot{R}^{-1} dR. \tag{50}$$

Upon numerical evaluation of the above integrals, one encounters difficulties due to singularities of $\dot{R}^{-1}$ at $R = R_{\min}$ and $R = R_{\max}$. This can be dealt with by employing Taylor expansions of $R(t)$ around $t=0$ and $t=T/2$, setting $R(0) = R_{\min}$. At the lower integration boundary, this gives

$$R(\Delta t) = R_{\min} + \tfrac{1}{2}\ddot{R}(0)\Delta t^2 + \mathcal{O}(\Delta t^3). \tag{51}$$

Then, by the Rayleigh–Plesset equation, $\ddot{R}(0) = F(R_{\min}, R_0, C_p)/R_{\min}$, so finally,

$$\Delta t \approx \sqrt{\frac{2[R(\Delta t) - R_{\min}]R_{\min}}{F(R_{\min}, R_0, C_p)}}. \tag{52}$$

In a similar way, one finds at the upper integration boundary,

$$\Delta t \approx \sqrt{\frac{2[R_{\max} - R(T/2 - \Delta t)]R_{\max}}{F(R_{\max}, R_0, C_p)}}. \tag{53}$$

With these expressions, we have calculated the long time moment limits for $\sigma = 0.1$ and $\sigma = 0.7$. Figure 4 shows that the computed values agree with the results obtained from direct computation. In addition, we have numerically computed the PDF for both values of σ by using numerical integration of Eq. (32). The resulting PDFs are plotted in Fig. 6.

IV. SLOWLY DECAYING STATISTICAL EQUILIBRIUM

Equation (26) governs the long time, stationary, behavior of statistics of the inviscid (Hamiltonian) bubbles. Two non-Hamiltonian effects must be considered before applying it to real bubbles. The first is physical damping of bubble oscillations due to viscosity, liquid compressibility, and heat and

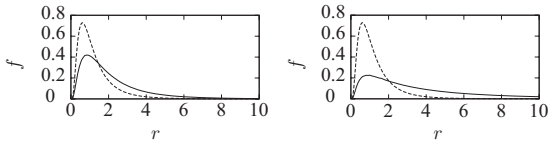

FIG. 6. Equilibrium PDF $f_r(r)$ (solid) and initial PDF $f(R_0)$ (dashed) for $\sigma=0.7$ and with $C_p=-0.84$ Ca (left) and $C_p=-0.999$ Ca (right).

mass transfer; we consider this effect in detail in this section. The second is nonimpulsive forcing of bubble oscillations, $C_p(t)$, which we discuss briefly in the last section.

For damping due to viscosity, liquid compressibility, and heat and mass transfer, which we collectively term "physical damping," unforced bubble oscillations ultimately decay to zero and each bubble reaches a static equilibrium (as opposed to a statistical one) with $R=R_0$. However, these physical damping mechanisms can, depending on the equilibrium radius, be weak compared to damping of bubble statistics associated with the approach to statistical equilibrium. In that case, bubbles may, on the time scale of damping, rapidly reach a statistical equilibrium. Thus, we may speak of a slowly varying statistical equilibrium where physical damping causes the equilibrium statistics to slowly decay to the static ones (i.e., the original distribution of equilibrium radius).

Below, we show that for typical broad distributions of equilibrium radii with most bubbles in the range of $1-100$ μm, these physical damping effects are indeed acting more slowly than the approach to statistical equilibrium. We thus consider a multiple-scale approach to Eq. (26), which we informally write as

$$E(\Psi)(\tau)=\int_0^\infty f(R_0)\left[\frac{1}{T(R_0,\tau)}\int_{\tau-T(R_0,\tau)}^{\tau}\Psi[R(t,R_0)]dt\right]dR_0. \tag{54}$$

The period of bubble oscillation, T, in Eq. (54) is now a function of the slow time scale since physical damping and forcing lead to changes in T. For linearized dynamics, this variation can be analytically determined, whereas for the nonlinear case, it must be either estimated based on a locally inviscid approximation or directly measured from the solution at previous times.

In the next two sections, we empirically explore the accuracy of using Eq. (54) for linear and nonlinear bubble dynamics, respectively, and compare results to those obtained using its direct counterpart, Eq. (18). We use the lognormal distribution for R_0, with various values of σ. For each case presented below, we numerically integrate as many as 5000 bubbles with different R_0 and evaluate Eq. (18) using Simpson's rule with all 5000 points. For Eq. (54), we find that a Gauss–Hermite quadrature of the integral with as few as five the quadrature points (values of R_0) is sufficient to reproduce the same results once statistical equilibrium is achieved. Individual bubbles are integrated in time using an adaptive fifth-order Runge–Kutta time marching method with error control.

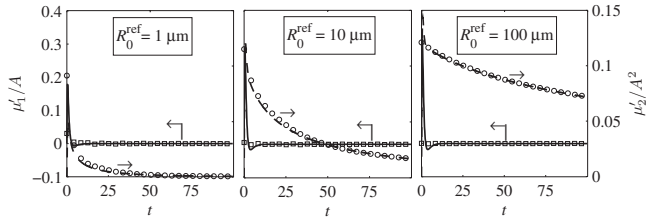

FIG. 7. Evolution of the first (—) and second (----) moments of bubble radius for the linearized viscous Rayleigh–Plesset equation. The lines denote direct quadrature of Eq. (18) and the symbols denote quadrature of Eq. (54). Lognormal distribution with $\sigma=0.7$ and various values of R_0^{ref}.

A. Linearized dynamics

We first consider linearized bubbles where physical damping is restricted to liquid viscosity, i.e., bubbles are governed by Eq. (13). The period, $T(R_0)$, appearing in Eq. (54) is independent of τ in the linear case and is analytically found.[32] Bubbles are initialized in static equilibrium (at $C_p=0$) and then impulsively forced according to

$$C_p=-A\exp\left[-\left(\frac{t}{T_f}\right)^2\right], \tag{55}$$

with T_f chosen sufficiently small to ensure that the dynamics are independent of T_f. For the linearized case, the value of A is irrelevant.

In Fig. 7, we show the evolution of $\mu_k'(t)$ for $k=1$ and 2, for $\sigma=0.7$, and R_0^{ref} of 1, 10, and 100 μm. For linear bubbles in statistical equilibrium, $\mu_1'(t)\to 0$. In all cases, this is rapidly achieved. For inviscid bubbles in statistical equilibrium, $\mu_2'(t)$ would approach a finite value, and its decay in Fig. 7 is the result of physical damping, which is strongest for the distribution of smaller bubbles. Despite the physical damping of the bubbles, the statistical equilibrium is rapidly achieved and the period-averaged formula (with just five quadrature points) is very accurate. The largest discrepancy occurs for the distribution of smaller bubbles as would be expected.

The quadrature error for both formulas is found by comparing the values of the integrals with varying the number of quadrature points to their values using a far-larger number and plotted in Fig. 8 for $R_0^{ref}=10$ μm. The integrand is also plotted for both cases to aid in interpreting the results. We

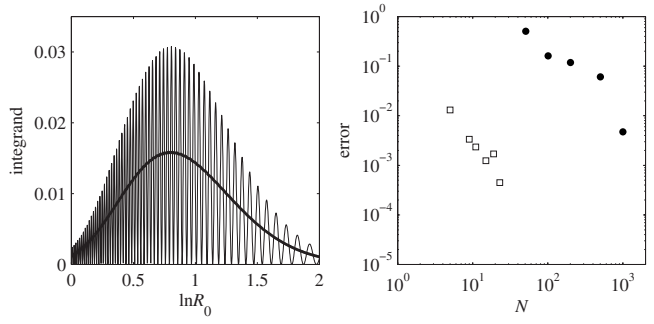

FIG. 8. Integrand (at left) and quadrature error (at right) for $\mu_2(t=100.0)$ for Eq. (18) (thin line and circle) and Eq. (54) (thick line and square) for the linearized, viscous Rayleigh–Plesset equation. Lognormal distribution with $R_0^{ref}=10$ μm and $\sigma=0.7$.

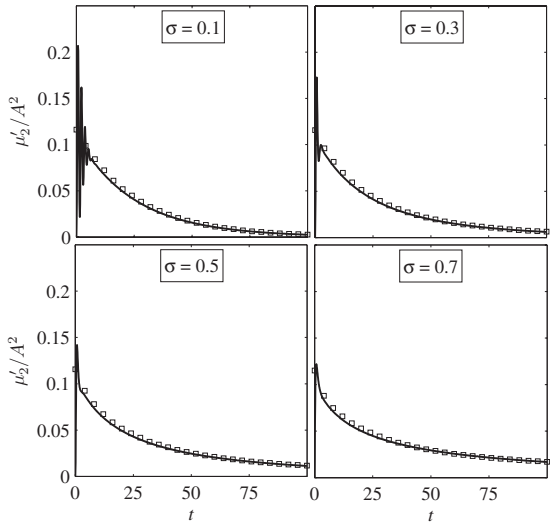

FIG. 9. Evolution of the $\mu_2'(t)$ for the linearized, viscous Rayleigh–Plesset equation. The lines denote direct quadrature of Eq. (18) and the symbols denote quadrature of Eq. (54). Lognormal distribution with $R_0^{\text{ref}}=10$ μm and various values of σ.

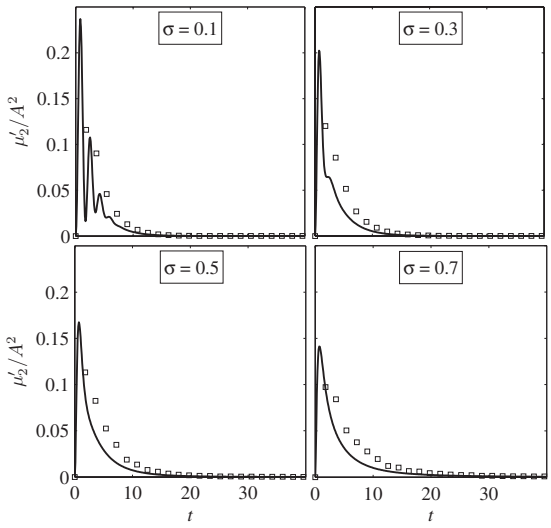

FIG. 11. Evolution of the $\mu_2'(t)$ for linearized model including compressibility and heat transfer for $R_0^{\text{ref}}=10$ μm. The lines denote direct quadrature of Eq. (18) and the symbols denote quadrature of Eq. (54).

see that the period averaging effectively removes oscillatory behavior from the integrand, resulting in accurate quadrature with far fewer points. For a reasonable accuracy, of about 1%, just five Gauss–Hermite points are needed to accurately integrate the period-averaged integrand; this number of quadrature points is used for all results that follow. We note that while the Gauss–Hermite quadrature should be optimal for integrals involving the lognormal distribution (we evaluate them using the log of R_0 as the independent variable), we do not achieve spectral convergence likely owing to lack of smoothness in the integrand, which is numerically determined by time marching each bubble. Nevertheless, we do find that the error for the Gauss–Hermite quadrature is far smaller for small numbers of bubbles than equally spaced quadrature points. On the other hand, to accurately evaluate the integrand in Eq. (18), we require as many as 5000 quadrature points. For that case, we use evenly spaced quadrature points (with Simpson's rule) since the Gauss–Hermite quadrature suffers from severe roundoff errors with more than about 40 quadrature points.

In Fig. 9, we vary the width of the lognormal distribution, $0.1<\sigma<0.7$. Again, the period-averaged formula is accurate for the entire range. We remark that in the limit of $\sigma\to 0$, statistical equilibrium is never achieved, bubble statistics approach zero only as a result of viscosity. For reference, in Fig. 10, we compare the early-time decay of μ_2' with $0.1<\sigma<0.7$ to a single 10 μm bubble, i.e., the case $\sigma=0$. It is clear that the damping due to viscosity acts more slowly than approach to statistical equilibrium for all $\sigma>0.1$.

In Fig. 11, we again vary the width of the lognormal distribution, but this time for the (linearized) bubble model that includes heat transfer and liquid compressibility. The period-averaged formula continues to hold for the more complicated model despite the much stronger physical damping associated with compressibility and heat transfer, which causes the bubble oscillations to rapidly decay to zero. For reference, we plot in Fig. 12 a distribution of larger bubbles, $R_0^{\text{ref}}=100$ μm, for which compressibility and heat transfer are less effective.

In summary, all the linear cases we tried show the efficacy of the period-averaged formula, Eq. (54), even when the

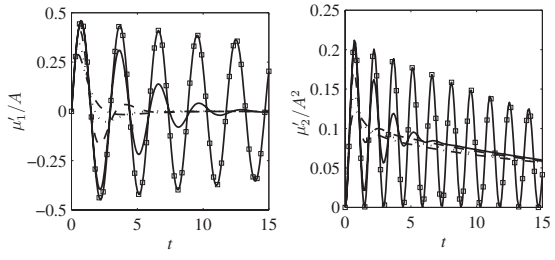

FIG. 10. Initial decay of the $\mu_1'(t)$ and $\mu_2'(t)$ for the linearized, viscous Rayleigh–Plesset equation, computed with Eq. (18). Lognormal distribution with $R_0^{\text{ref}}=10$ μm and $\sigma=0$ (— with square), $\sigma=0.1$ (—), $\sigma=0.3$ (----), $\sigma=0.5$ (···), and $\sigma=0.7$ (–·–).

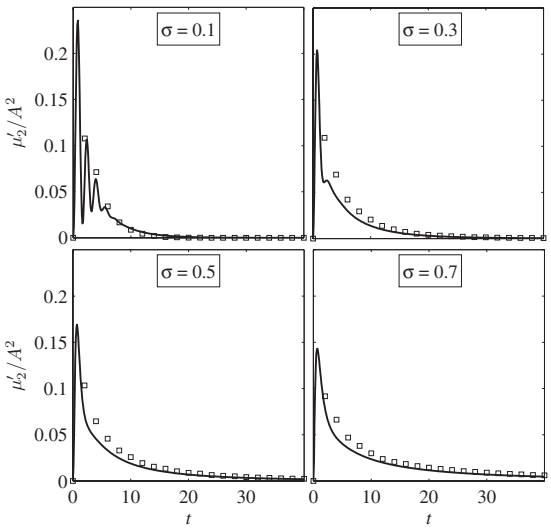

FIG. 12. Same as in Fig. 11 but with $R_0^{\text{ref}}=100$ μm.

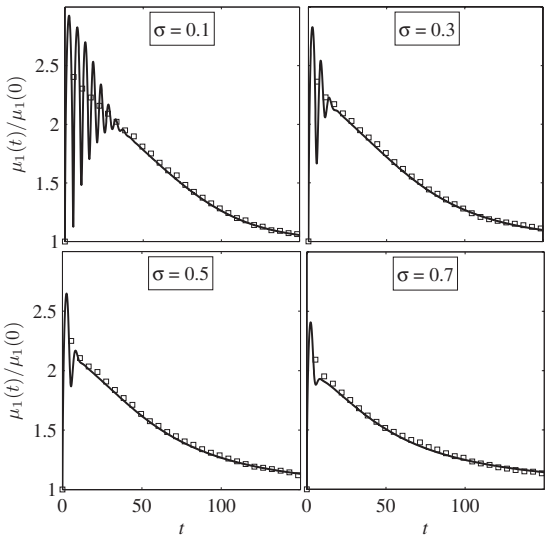

FIG. 13. Evolution of the $\mu_1(t)$ for the nonlinear, viscous Rayleigh–Plesset equation with $R_0^{\mathrm{ref}}=10$ μm and $A=4$. The lines denote direct quadrature of Eq. (18) and the symbols denote quadrature of Eq. (54).

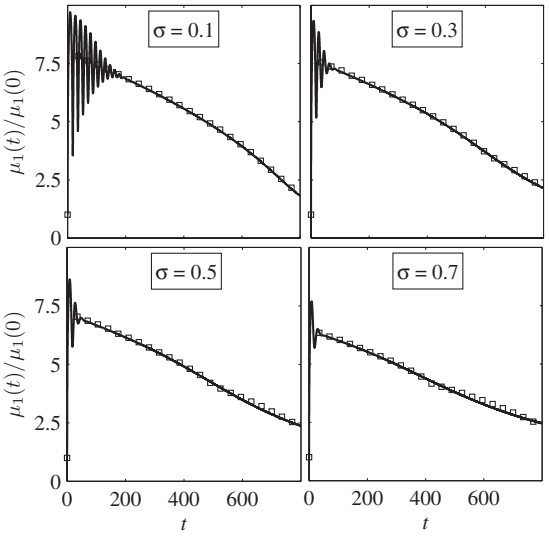

FIG. 14. Same as in Fig. 13 but with $A=25.0$.

effects of physical damping of bubble are quite strong. In all cases, it was sufficient to integrate only five bubbles in order to accurately predict the statistics.

B. Application to nonlinear dynamics

In the nonlinear case, we do not have an available explicit expression for the period T, and therefore, the period T has to be numerically calculated. By using Eq. (50), we numerically calculated T for a wide range of values of R_0, C_p, and $\mathcal{H}$, and the results have been stored in a database which can be used as a look-up table during the bubble-dynamic computations.

We consider the nonlinear Rayleigh–Plesset equation. Bubbles are again impulsively forced with Eq. (55), but the value of A has a strong impact on the resulting bubble dynamics in the nonlinear case. We examine two cases where A has been chosen as 4 and 25 in order to cause a bubble with $R_0^{\mathrm{ref}}=10$ μm to grow to three and ten times its equilibrium radius, respectively. These values are indicative of strongly nonlinear bubbles.

In Figs. 13 and 14, we show the results for $\mu_1(t)$ with $A=4$ and 25, respectively. For the lowest values of $\sigma=0.1$ and 0.3, we see a more pronounced initial transient where statistical equilibrium is not yet achieved than in the corresponding linear case. Note that the bubble oscillation period for the nonlinear case is longer than the corresponding linear cases. Nevertheless, we again find in both cases that during statistical equilibrium, bubble statistics are very well approximated by Eq. (54) with just five quadrature points for these nonlinear physically damped bubbles. In Fig. 15, other relevant moments are shown for the case where $A=8$, including moments that would be needed to close bubble flow equations such as $\mu_{-1}(t)$ and $\mu_3(t)$, the latter being particularly important as it is proportional to the void fraction. Apparently Eq. (54) is equally valid for all relevant moments.

V. SUMMARY AND EXTENSIONS

The main result of this paper is that once a distribution of inviscid, oscillating bubbles reaches a stationary equilibrium, moments of the bubble radius may be found by replacing the bubble radius with its period-averaged value. Provided the PDF of equilibrium radius is sufficiently broad, the time scale required to reach statistical equilibrium is short compared to the physical damping of bubbles by viscosity, heat transfer, and liquid compressibility, at least for equilibrium radius distributions that are likely to occur in practical situations, where equilibrium radius can vary over a few orders of magnitude with average values in the range of $1-100$ μm. In these cases, it is also permissible to replace the bubble radius with its period-averaged value when computing moments of the radius distribution.

A major benefit of the result is that the period-averaged bubble radius is a much smoother function of the equilibrium

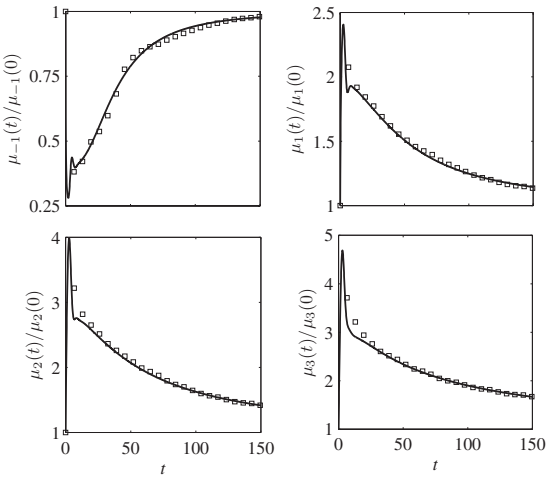

FIG. 15. Evolution of the μ_{-1}, μ_1, μ_2, and μ_3 for the nonlinear, viscous Rayleigh–Plesset equation with $R_0^{\mathrm{Ref}}=10$ μm, $A=4.0$, and $\sigma=0.7$. The lines denote direct quadrature of Eq. (18) and the symbols denote quadrature of Eq. (54).

radius than is the bubble radius itself. We showed in specific examples of linear and nonlinear bubble oscillations that accurate statistics could be computed by tracking as few as five individual period-averaged bubbles compared to $O(1000)$ that are required for a direct computation. The computational savings means that continuum bubbly flow models can be implemented for more complex flows while, at the same time, accounting for the important effect of size distribution of equilibrium radius.

Important aspects of this problem require further investigation before the period-averaged formula can be used for more general problems involving continual forcing of bubbles either through a specified nonimpulsive $C_p(t)$ or through two-way coupling with the flow. Certain cases, such as when bubbles are slowly forced compared to bubble period, should allow moments of the distribution to be computed with the period-averaged value since filtering the response over the bubble period will have little effect on the moments. A more serious challenge is forcing or coupling that leads to unstable growth of bubbles whose radius exceeds the Blake critical radius or that leads to resonance of particular bubbles. It may, for example, be possible to isolate resonating bubbles, say, at the forcing frequency and its harmonics and subharmonics, and individually track these bubble contributions to the moments. We hope to address these issues in a future work.

ACKNOWLEDGMENTS

The authors would like to express their thanks to Dr. Rutger IJzermans for his observations about Eq. (18). T.E.C. gratefully acknowledges support by NIH Grant No. PO1 DK43881 and ONR Grant No. N00014-06-1-0730. R.H. worked on this paper while visiting Caltech. He gratefully acknowledges support by Caltech and the University of Twente.

APPENDIX: SPHERICAL BUBBLE DYNAMICS INCLUDING LIQUID COMPRESSIBILITY AND HEAT TRANSFER

To illustrate the applicability of statistical equilibrium computations to more complex spherical bubble-dynamic models, we consider a simple model that includes, in an approximate way, the effects of liquid compressibility and heat transfer. For reference, we list here the assumptions and equations governing the model. To be clear, we are not asserting that the model discussed here is accurate in all situations; the references given below should be consulted for full details. Rather, we take the model as representative of models that introduce significant bubble damping due to compressibility and heat transfer.

The model assumes that (a) the mass of noncondensable gas in the bubble remains constant, (b) the liquid is cold (far from boiling point), (c) phase change instantaneously occurs, and (d) the bubble contents have a spatially uniform pressure (homobaric). These assumptions are typically adequate except near the end of a violent bubble collapse, see, for example, Refs. 22–29. With these assumptions, internal bubble pressure p_b (sum of vapor pressure and noncondensable gas pressure) is governed by an ODE,

$$\dot{p}_b = \frac{3\gamma}{R}\left[-\dot{R}p_b + \mathcal{R}_v \dot{m}_v'' T_w + p_{b0}\frac{k_{mw}}{\mathrm{Pe}_T}\frac{1}{R}\left.\frac{\partial T}{\partial y}\right|_w \right], \tag{A1}$$

where γ is the specific-heat ratio of noncondensable gas and vapor ($\gamma_n \approx \gamma_v \equiv \gamma$), R is the radius, T is the temperature, $\mathcal{R}_v$ is the gas constant, $\dot{m}''$ is the mass flux at the bubble wall, k is the thermal conductivity, and y is the normalized radial coordinate. $\mathrm{Pe}_T = \sqrt{(p_0/\rho_0)}(R_0^{\mathrm{ref}}/\alpha_0)$ is the Peclet number for heat transfer, where α_0 is the (heat) diffusivity of the equilibrium bubble contents. Finally, the subscripts 0 and w denotes initial, equilibrium conditions and bubble wall properties, respectively; the subscripts m, v, and n denote quantities for the mixture, the vapor, and the noncondensable gas, respectively. Representative values of Pe_T for bubbles with sizes 1, 10, and 100 μm are given in Table I.

The nondimensionalization used here is the same as discussed in Sec. II A, with the addition of a reference temperature T_0, which is taken as the ambient liquid temperature. Liquid properties and the transport properties of individual gas components are assumed constant, and the thermal conductivity for the gas mixture is taken from a semiempirical formula.[33]

The bubble internal phenomena that govern the diffusion processes are so complex that the simple polytropic assumption for the noncondensable gas is inadequate. Preston *et al.*[29] employed constant transfer coefficients to estimate the heat and mass flux at the bubble wall,

$$\left.\frac{\partial \chi_v}{\partial y}\right|_w \approx -\beta_\chi(\overline{\chi_v} - \chi_{vw}), \qquad \left.\frac{\partial T}{\partial y}\right|_w \approx -\beta_T(\bar{T} - T_w), \tag{A2}$$

where the overbar denotes the volume average over the bubble, χ_v denotes the mass fraction of vapor, and the constant transfer coefficients are approximated by

$$\beta = \frac{1}{2}\left[\left(\sqrt{iR_0^2\omega_N \mathrm{Pe}}\coth\sqrt{iR_0^2\omega_N \mathrm{Pe}} - 1\right)^{-1} - \frac{3}{iR_0^2\omega_N \mathrm{Pe}}\right]^{-1} + \text{c.c.}, \tag{A3}$$

where Pe_T is used for β_T, and $\mathrm{Pe}_\chi = \sqrt{(p_0/\rho_0)}(R_0^{\mathrm{ref}}/\mathcal{D}_0)$, the Peclet number for mass transfer ($\mathcal{D}_0$ is the diffusivity between water vapor and noncondensable gas), is used for β_χ. ω_N is the bubble natural frequency. In the linear scenario, the model is exact as the Peclet numbers approach zero. The model has been shown to be very accurate for nonlinear bubble dynamics provided the bubble growth is not too large ($R_{\max}/R_0 < \sim 10$). Note that β_T can be set to zero to recover adiabatic behavior for the noncondensable gas, and β_χ can be set to zero for noncavitating gas bubbles.

To approximately account for liquid compressibility, we employ Gilmore's model[30] (see also (Refs. 34 and 35),

$$R\ddot{R}\left(1-\frac{\dot{R}}{a}\right)+\frac{3}{2}\dot{R}^2\left(1-\frac{1}{3}\frac{\dot{R}}{a}\right)=H\left(1+\frac{\dot{R}}{a}\right)+\frac{R\dot{H}}{a}\left(1-\frac{\dot{R}}{a}\right), \tag{A4}$$

where H and A are the enthalpy and speed of sound, respectively, at the bubble wall in the liquid, nondimensionalized with the characteristic velocity $\sqrt{p_0/\rho_0}$,

$$H=\frac{n(1+B)}{n-1}\left[\left(\frac{C_b}{1+B}+1\right)^{(n-1)/n}-\left(\frac{C_p}{1+B}+1\right)^{(n-1)/n}\right], \tag{A5}$$

$$a=\sqrt{n(1+B)\left(\frac{C_p}{1+B}+1\right)^{(n-1)/n}+(n-1)H}. \tag{A6}$$

Here, n and B are the nondimensional numerical constants from the Tait equation of state for water, $n=7.15$, and $B=3009$. C_b is the pressure coefficient at the bubble wall in the liquid and is given by

$$C_b=p_b-1-\frac{4}{\mathrm{Re}}\frac{\dot{R}}{R}-\frac{2}{\mathrm{We}R}. \tag{A7}$$

In the incompressible limit, the Gilmore equation (A2) recovers the well-known incompressible Rayleigh–Plesset equation.

Finally, assuming that Fick's law holds for mass diffusion between vapor and noncondensable gas, the species conservation requires

$$\dot{m}_v''=\frac{\rho_{mw}}{Pe_\chi(1-\chi_{vw})R}\frac{\partial\chi_v}{\partial y}. \tag{A8}$$

By using the perfect gas law, ρ_{mw} and χ_{vw} are given by

$$\chi_{vw}=\left[1+\frac{\mathcal{R}_v}{\mathcal{R}_n}\left(\frac{p_b}{p_v}-1\right)\right]^{-1}, \tag{A9}$$

$$\rho_{mw}=\frac{p_v}{\chi_{vw}\mathcal{R}_vT_w}. \tag{A10}$$

Note that T_w is constant ($T_w=T_0$) by the cold liquid assumption.

As a direct result of the four assumptions, (a)–(d), and the constant transfer model, there is no need to solve any PDEs for the conservation laws in either liquid or gas phase; rather, two ODEs, Eqs. (A1) and (A2) are solved with the constraint (A8).

[1] D. Z. Zhang and A. Prosperetti, "Ensemble phase-averaged equations for bubbly flows," Phys. Fluids **6**, 2956 (1994).
[2] A relative velocity between the bubble and mixture velocity may also be included.
[3] L. van Wijngaarden, "On the equations of motion for mixtures of liquid and gas bubbles," J. Fluid Mech. **33**, 465 (1968).
[4] A. Biesheuvel and L. van Wijngaarden, "Two phase flow equations for a dilute dispersion of gas bubbles in liquid," J. Fluid Mech. **148**, 301 (1984).
[5] R. E. Caflisch, M. J. Miksis, C. Papanicolaou, and L. Ting, "Effective equations for wave propagation in bubbly liquids," J. Fluid Mech. **153**, 259 (1985).
[6] We refer to Ref. 1 for detailed comparisons of the different models.
[7] K. Commander and A. Prosperetti, "Linear pressure waves in bubbly liquids: Comparison between theory and experiments," J. Acoust. Soc. Am. **85**, 732 (1989).
[8] L. Noordzij and L. van Wijngaarden, "Relaxation effects, caused by relative motion, on shock waves in gas bubble/liquid mixtures," J. Fluid Mech. **66**, 115 (1974).
[9] R. Omta, "Oscillations of a cloud of bubbles of small and not so small amplitude," J. Acoust. Soc. Am. **82**, 1018 (1989).
[10] P. Smereka and S. Banerjee, "The dynamics of periodically driven bubble clouds," Phys. Fluids **31**, 3519 (1988).
[11] L. d'Agostino, C. E. Brennen, and A. J. Acosta, "Linearized dynamics of two-dimensional bubbly and cavitating flows over slender surfaces," J. Fluid Mech. **192**, 485 (1988).
[12] G. E. Reisman, Y. C. Wang, and C. E. Brennen, "Observations of shock waves in cloud cavitation," J. Fluid Mech. **355**, 255 (1998).
[13] Y.-C. Wang and C. Brennen, "One-dimensional bubbly cavitating flows through a converging-diverging nozzle," J. Fluids Eng. **120**, 166 (1998).
[14] Y.-C. Wang, "Effects of nuclei size distribution on the dynamics of a spherical cloud of cavitation bubbles," J. Fluids Eng. **121**, 881 (December 1999).
[15] A. T. Preston, T. Colonius, and C. E. Brennen, "A numerical investigation of unsteady bubbly cavitating nozzle flows," Phys. Fluids **14**, 300 (2002).
[16] M. Tanguay, "Computation of bubbly cavitating flow in shock wave lithotripsy," Ph.D. thesis, California Institute of Technology (2004).
[17] C. E. Brennen, *Cavitation and Bubble Dynamics* (Oxford University Press, New York, 1995).
[18] J. Ma and P. Wang, "Effects of initial air content on the dynamics of bubbles in liquids," IBM J. Res. Dev. **6**, 472 (1962).
[19] H. Chang and L. Chen, "Growth of a gas bubble in a viscous fluid," Phys. Fluids **29**, 3580 (1986).
[20] Z. Feng and L. Leal, "Nonlinear bubble dynamics," Annu. Rev. Fluid Mech. **29**, 201 (1997).
[21] G. Batchelor, *An Introduction to Fluid Dynamics* (Cambridge University Press, New York, 1967).
[22] M. Plesset and A. Prosperetti, "Bubble dynamics and cavitation," Annu. Rev. Fluid Mech. **9**, 145 (1977).
[23] S. Fujikawa and T. Akamatsu, "Effects of the non-equilibrium condensation of vapor on the pressure wave produced by the collapse of a bubble in a liquid," J. Fluid Mech. **97**, 481 (1980).
[24] A. Prosperetti, L. A. Crum, and K. W. Commander, "Nonlinear bubble dynamics," J. Acoust. Soc. Am. **83**, 502 (1988).
[25] M. Watanabe and A. Prosperetti, "Shock waves in dilute bubbly liquids," J. Fluid Mech. **274**, 349 (1994).
[26] M. Ichihara, H. Kawashima, and M. Kameda, "Dynamics of a spherical gas/vapor bubble," *Proceedings of 2000 Japan-US Multiphase Flow Seminar*, June 5-8, 2000, Santa Barbara, California.
[27] R. Toegel, B. Gompf, R. Pecha, and D. Lohse, "Does water vapor prevent upscaling sonoluminescence?," Phys. Rev. Lett. **85**, 3165 (2000).
[28] B. D. Storey and A. J. Szeri, "A reduced model of cavitation physics for use in sonochemistry," Proc. R. Soc. London, Ser. A **457**, 1685 (2001).
[29] A. T. Preston, T. Colonius, and C. E. Brennen, "A reduced-order model of diffusive effects on the dynamics of bubbles," Phys. Fluids **19**, 123302 (2007).
[30] F. Gilmore, "The collapse and growth of a spherical bubble in a viscous compressible liquid," California Institute of Technical Hydrodynamic Laboratory Technical Report No. 26-4 (1952).
[31] A. Erdelyi, *Asymptotic Expansions* (Dover, New York, 1956).
[32] In the case of the model including liquid compressibility and heat transfer, the period may still be analytically found, but for convenience, we simply measured the period in the solutions for each R_0 by finding the time between consecutive minimum values.
[33] R. Bird, W. Stewart, and E. Lightfoot, *Transport Phenomena* (Wiley, New York, 1960).
[34] R. Hickling and M. S. Plesset, "Collapse and rebound of a spherical bubble in water," Phys. Fluids **7**, 7 (1964).
[35] A. Prosperetti and A. Lezzi, "Bubble dynamics in a compressible liquid. Part 1. First-order theory," J. Fluid Mech. **168**, 457 (1986).